ChemComm

Accepted Manuscript

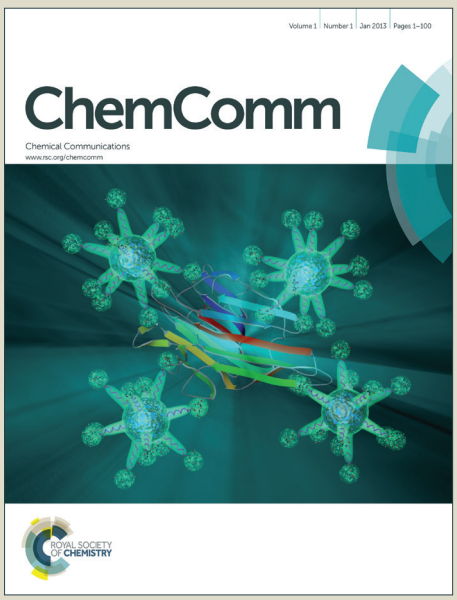

This is an *Accepted Manuscript*, which has been through the Royal Society of Chemistry peer review process and has been accepted for publication.

Accepted Manuscripts are published online shortly after acceptance, before technical editing, formatting and proof reading. Using this free service, authors can make their results available to the community, in citable form, before we publish the edited article. We will replace this *Accepted Manuscript* with the edited and formatted *Advance Article* as soon as it is available.

You can find more information about *Accepted Manuscripts* in the Information for Authors.

Please note that technical editing may introduce minor changes to the text and/or graphics, which may alter content. The journal's standard Terms & Conditions and the Ethical guidelines still apply. In no event shall the Royal Society of Chemistry be held responsible for any errors or omissions in this *Accepted Manuscript* or any consequences arising from the use of any information it contains.

ROYAL SOCIETY OF CHEMISTRY

www.rsc.org/chemcomm

ChemComm

RSCPublishing

COMMUNICATION

Morphological tuning *via* structural modulations in AIE luminogens with least possible variables and their use in live cell imaging

Cite this: DOI: 10.1039/x0xx00000x

Received ooth January 2012,
Accepted ooth January 2012

DOI: 10.1039/x0xx00000x

www.rsc.org/

Roop Shikha Singh,[a] Rakesh Kumar Gupta,[a] Rajendra Prasad Paitandi,[a] Mrigendra Dubey,[a] Gunjan Sharma,[b] Biplob Koch[b] and Daya Shankar Pandey*[a]

With intent to fine tune the morphological and photophysical properties, three novel AIE luminogens (BQ1–BQ3) based on quinoline-BODIPY have been synthesized. Judicious choice of substituents (–H, $–CH_3$, $–OCH_3$) in these systems led to nanoballs in BQ1 and BQ2 while reticulated nanofibers in BQ3 along with diverse photophysical behaviour.

The discovery of aggregation induced emission (AIE) by Tang *et al,* was much of a surprise, since it challenged our general perception about luminescence, as organic luminophores witnessed a downfall in their potential applications due to aggregation caused quenching (ACQ) effect.[1] This revelation followed development of numerous excellent AIE luminophores based on tetraphenylethene, cyanostilbene, 9,10-distyrylanthracene, benzoxazoles etc.[2] The phenomenon of AIE can be related to restricted intramolecular rotation (RIR), reduced co-facial intermolecular π overlap, specific molecular arrangements such as *J*-aggregation, or dimer stacking and intramolecular charge transfer (ICT).[3] Lately, some fluorescent dyes with a variety of functionalities have been designed on AIE platform to illustrate promising applications in photonic biosensors and nanomaterials.[4] Among these, boron-dipyrromethenes (BODIPYs) have been fascinating because of their resourceful applications in light harvesting antenna system, solar cell sensitizers, molecular photonic wires, fluorescent switches, marker and sensors in contemporary chemistry and biology.[5] Despite being excellent emitters in solution, the BODIPY dyes hardly fluoresces in solid state due to severe self-quenching arising from small Stokes shift and planar π–conjugated structures. To expand their technological applications, current research has seen a large surge in overcoming weaknesses of the BODIPY dyes by introducing sterically bulky substituents to inhibit close packing.[2a,6]

Apart from being good metal chelators, functionalized quinolines are highly emissive in solution as well as in solid state with high quantum yield, good electron transport and excited state intra-molecular proton transfer (ESIPT).[7] Although these serve as good candidates for fluorescent dyes, molecular sensors, construction of D–A architecture and fluorescent markers in biological systems,[8] AIE active quinoline derivatives have scantly been reported.[9] These facts prompted us to hypothesize that it might be beneficial to use quinoline-BODIPY as a platform to investigate AIE.

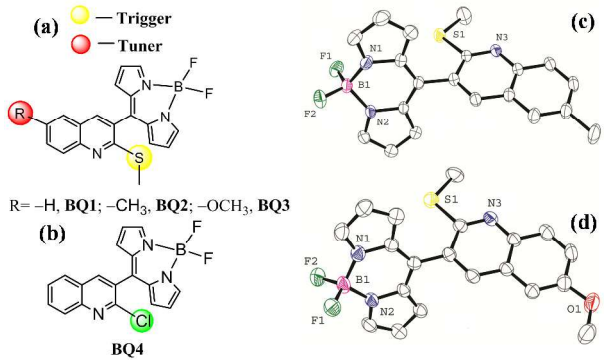

Fig. 1 Chemical structures of **BQ1**–**BQ3** (a), **BQ4** (b) and ORTEP views of **BQ2** (c), **BQ3** (d) at *40%* ellipsoidal probability.

Although photonics of the AIE luminogens have been investigated extensively, due attention toward strategies leading to aggregates and their morphology has been wanting. Developing an approach that could address aforesaid issues without conventional decorated luminophores has been challenging. With an intention of tuning the morphology of aggregates and their optical properties *via* minimum possible variations, three novel AIE luminogens have been designed using quinoline-BODIPY as a platform. Strategically, thioether ($–SCH_3$) group has been used as triggering unit and to tune the AIE, a tuner varying from hydrogen (**BQ1**), methyl (**BQ2**) to methoxy group (**BQ3**) placed diagonal to $–SCH_3$ group. Sulfur containing group has been chosen as sulfur can increase the intra- and intermolecular electronic motion due to its high polarizability. In addition, to affirm triggering effect of $–SCH_3$, a model compound having –Cl in its place has also been synthesized (**BQ4**). Further, to restrict rotation of the quinoline unit around BODIPY core triggering unit has been placed in

ChemComm Accepted Manuscript

close proximity to the quinoline nitrogen wherein $-SCH_3$ being bulkier than –Cl imposes greater steric hindrance (Fig. 1). This approach offered clear implication of the steric hindrance on RIR as **BQ1**–**BQ3** are AIE active, while **BQ4** is inactive in this regard (Fig. S 16). It is well documented that various interactions in the solid state play an essential role in aggregation and AIE. However, their utility in determining shape of the aggregates needs to be scrutinized as these offer information about distribution of the hydrophilic and hydrophobic moieties. Therefore, hydrogen (**BQ1**) has been chosen as tuner for obvious reasons, methyl group (**BQ2**) as a weak electron donor that also maintains hydrophobicity in the quinoline core, while methoxy group (**BQ3**) as an electron donating group that renders some hydrophilicity to the quinoline moiety.

Dipyrromethanes **5**–**8** have been prepared by condensation of the aldehydes **1**–**4** with an excess of pyrrole in presence of catalytic amounts of trifluoroacetic acid. The BODIPYs **BQ1**–**BQ4** has been synthesized by reacting respective dipyrrins, obtained *in-situ* by oxidation of **5**–**8** using DDQ, with $BF_3{\cdot}Et_2O$ in presence of Et_3N (ESI†). Elemental analyses, IR, NMR (^1H, ^{13}C), HRMS, electronic absorption, and emission spectroscopic studies well supported their proposed formulations. Structures of **BQ1**–**BQ4** have unambiguously been authenticated by X-ray single crystal analyses (Fig. S1–S10, S26, ESI†).

Optical properties of BODIPYs **BQ1**–**BQ4** have been investigated in methanol. These displayed typical absorption bands associated with BODIPY[6c,10] at ~ 507 nm due to π–π* transitions along with a high energy band corresponding to n–π* at ~ 340 nm (*c*, 50 μM) (Fig. S11a, ESI†). Illumination of **BQ1**–**BQ4** at ~ 340 nm resulted in dual emission due to quinoline and BODIPY moieties at 435 and 530 nm, respectively. However, upon excitation at 507 nm it gave an emission band solely due to BODIPY unit (Fig. S11b, 12, ESI†). Excitation spectra of these compounds have been monitored at both emission bands which supported the origin of dual emission (Fig. S13, ESI†). Absorption and emission spectra of **BQ1**–**BQ4** have also been acquired in solvents with varying polarities. Notably, these compounds exhibited lower fluorescence intensity in polar solvents relative to apolar ones except for **BQ4** (Fig. S19–S21, ESI†). On the other hand, absorption spectra did not show any significant change. This behaviour reflected some polarization of the emissive state whereas ground state was unaffected.

Being excellent chromophores, BODIPYs are expected to exhibit fascinating photophysical properties in methanol/water mixture (*c*, 50 μM) of varying compositions. **BQ1**–**BQ3**, in their UV-vis spectra, displayed almost identical absorption profiles with increasing water content while **BQ4** exhibited insignificant changes. Upon addition of water upto 90%, **BQ1**–**BQ3** showed a decrease in absorbance along with a level-off tail in the visible spectral region, a common feature of the nanoaggregate suspension.[11] Remarkably, colour of the solution also turned red from yellow (Fig. S14-15, S22, ESI†). It may be attributed to an increase in π–π interactions, thereby, creation of the nanoaggregates. To substantiate aggregation process photoluminescence (PL) of **BQ1**–**BQ3** has been acquired using aforesaid solvent system. Unlike absorption, PL spectra displayed significant variations wherein **BQ1**–**BQ3** showed emission bands at ~435 and ~532 nm. Intensity of both the bands diminished with increasing water fraction (f_w), and solution became almost nonluminescent at f_w <70%. In **BQ1** and **BQ2** two peaks emerged at 571 and 612 nm as the water content exceeded 70%, which intensified with increasing water content and attained maximum value at f_w 90% (Fig. 2a, S17–18, ESI†), whereas emission band corresponding to quinoline unit gradually disappeared.

However, for **BQ3** both the emission bands showed some unusual changes at f_w 70% (Fig. 2b), possibly due to progressive aggregation (Fig. S24, ESI†). Further additions of water quenched the emission at 532 nm with emergence of a new peak at 620 nm, which strengthened with greater water content and attained maxima at f_w 90% (Fig. 2b). It is noteworthy to mention that at f_w 90% **BQ1** displayed emission in aggregated state without any enhancement, whereas 4- and 2-fold enhancement in fluorescence intensity was observed for **BQ2** and **BQ3,** respectively. Water being poor solvent promotes aggregation of these molecules at f_w > 70% and RIR resulted in an enhanced fluorescence (AIE). Apparently all these compounds displayed red shift upon aggregation, a frequently observed feature in AIE systems.[2–4] Multiple emission bands upon aggregation may arise due to presence of both monomeric and aggregated state in solution.[6b] Striking variation in the emission pattern and AIE for **BQ1**–**BQ3** advocated profound substituent effect and if implicit assumptions are right, this would affect morphology of the aggregates as well.

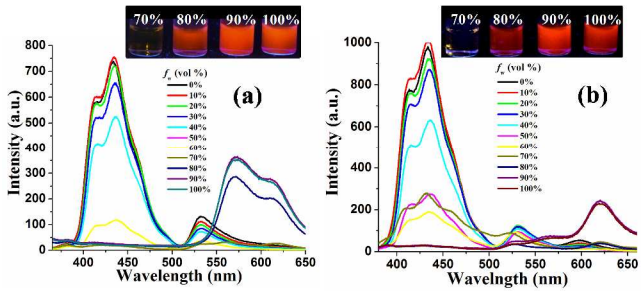

Fig. 2 Fluorescence spectra of **BQ2** (a) and **BQ3** (b) in methanol/water mixture (*c*, 50 μM) with different volume fractions of water (f_w).

To gain deep insight into aggregation and diverse optical behaviour, water–methanol (90%) mixtures of **BQ1**–**BQ3** were subjected to scanning electron, transmission electron and atomic force microscopy (SEM, TEM and AFM). It was observed that these created different types of nanoaggregates depending upon respective substituents. As it is clear from the images (Fig. 3, S23, ESI†) **BQ1** and **BQ2** gave nano-ball aggregates of uniform size with average diameter of 220 and 150 nm, **BQ3** formed a highly reticulated network of ~300 nm thick fibrous nanoaggregate. Smaller size of the aggregate in **BQ2** relative to **BQ1** may be due to greater hydrophobicity of **BQ2**. The TEM images displayed further assembly of aligned nanoballs in **BQ1** and **BQ2** (Fig. 3b, 3e). The shape and size of these aggregates are in good agreement with those obtained from the AFM (Fig. 3c, 3f and Fig. S23, ESI†). This morphological disparity strengthened and established the proposition that nanoaggregate morphologies are tunable by judiciously chosen substituents even using same platform and analogous conditions.

The morphological variation for aggregates from nanoballs to fibers and their discrete photophysical behaviour revealed significant role of strong directional intermolecular interactions. This prompted us to look into crystal structure of these compounds. Careful examination of the crystal structure of **BQ1** revealed that it lacks

ChemComm Accepted Manuscript

This journal is © The Royal Society of Chemistry 2012

π–π interactions and quinoline units of one molecule are inter-connected to the adjacent ones through C–H···π interactions (2.691 Å) in a slightly slipped manner (Fig. S27a, ESI†).

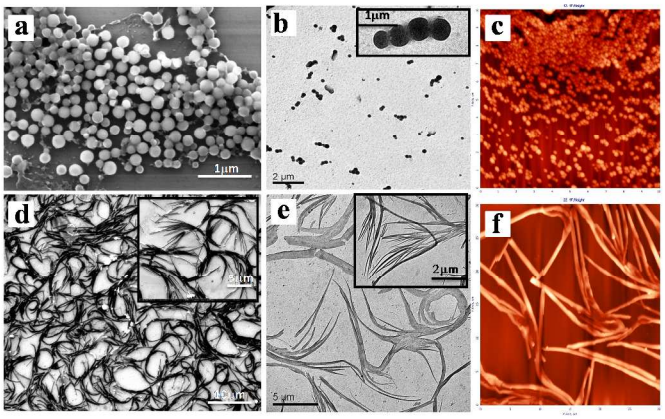

Fig. 3 SEM (a, d); TEM (b, e) and AFM (c, f) images of nanoball in **BQ2** (Top) and nanofiber in **BQ3** (Bottom) at *c*, 50 μM with f_w = 90%. Inset shows the corresponding magnified images.

BQ2 exists in a dimeric form where neighbouring dipyrromethene units are linked by face to face π–π interaction (3.353 Å; Fig. S28, ESI†). Rather larger slipped stacking in this molecule weakens the π–π interactions and favors *J*-aggregation. Whereas **BQ3** stacks in a herringbone mode through long-range ordered arrangement and forms a typical *J*-aggregate in which adjacent molecules are packed in anti parallel (head to tail) manner. The quinoline moiety of one molecule interacts with boron-dipyrrin moiety of the nearby molecule through π–π (3.397, 3.363 Å) and C–H···π (2.872, 2.810 Å) interactions (Fig. S30–32, ESI†). A closer look at hydrogen bonding interactions revealed that **BQ1** has one C–H···π (2.691 Å) and two face-to-face C–H···F interactions (Fig. S27 b, ESI†). Likewise, **BQ2** has one each of face-to-edge C–H···π (2.751 Å) and face-to-edge C–H···N (2.679 Å) interactions (Fig. S29, ESI†). On the other hand **BQ3** possesses two C–H···π (vide-supra) and two C–H···F (2.614) hydrogen bonding interactions all along the direction of the long molecular axis. (Fig. S31, ESI†). These interactions provide a rigid 3-D network and restrict intramolecular rotation of quinoline unit around the BODIPY core, thereby increasing the emission intensity in aggregated state. Aforesaid interactions also support the reason behind red shifts in **BQ1**–**BQ3** upon aggregation. **BQ3** experiences maximum red shift (90nm) followed by **BQ2** (81nm) and **BQ1** (79nm), as **BQ3** has minimum face to face interactions with adjacent units, hence weaker π–π interactions favoring *J*-aggregation.

The mechanism of aggregate build-up has been deduced considering dominance of the solid state interactions in aggregated state which has also been evidenced by powder XRD patterns (Fig. S25, ESI†). The anticipated out-turn of intermolecular interactions are profound as it brings distribution of the hydrophilic and hydrophobic domains in such a way that polar groups are exposed to aqueous environment shielding nonpolar groups away from water to form the hydrophobic core. With increasing water gradient, H-bonding interactions in **BQ1** and **BQ2** favor a nanoball wherein hydrophilic BF_2 unit comes outwards to maximize the interaction with water and quinoline unit forms hydrophobic core (Fig. 4). **BQ3** displays a self-assembled aggregate of twisted and highly branched fibers. It is endowed with two hydrophilic groups, methoxy and BF_2 units, which are well separated by hydrophobic quinoline unit. The aforesaid interactions bring hydrophilic groups on both sides of the fiber favoring a sideways aggregation *via* interaction with water (Fig. 4; Fig. S32, ESI†).

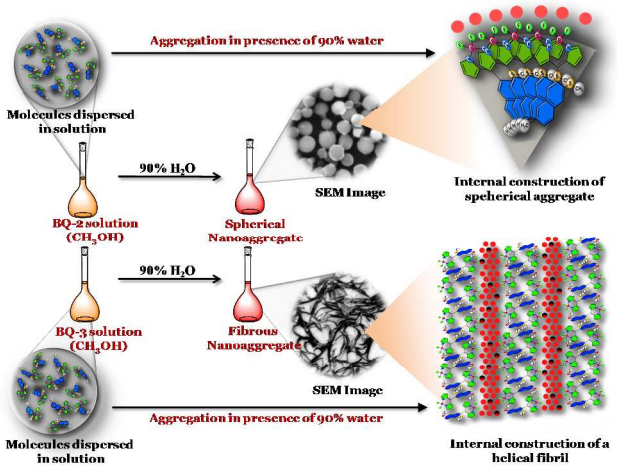

Fig. 4 Mechanistic interpretation of aggregation from randomly dispersed molecules to nanoaggregates in **BQ2** (top) and **BQ3** (bottom) upon increasing the water content (f_w = 90%): A cross sectional insight of nanoball in **BQ2** and nanofiber in **BQ3**.

To have better understanding of the spectroscopic results, theoretical calculations have been performed on energy levels of **BQ1**–**BQ3** (Fig. S33, ESI†). The HOMO energy levels are dominated by the orbitals from quinoline units while LUMO are concentrated on BODIPY core. The calculated HOMO–LUMO gaps for **BQ1**, **BQ2** and **BQ3** are 3.02, 3.02, 2.96 ev respectively, which are in good agreement with those obtained from UV-vis spectroscopic data.

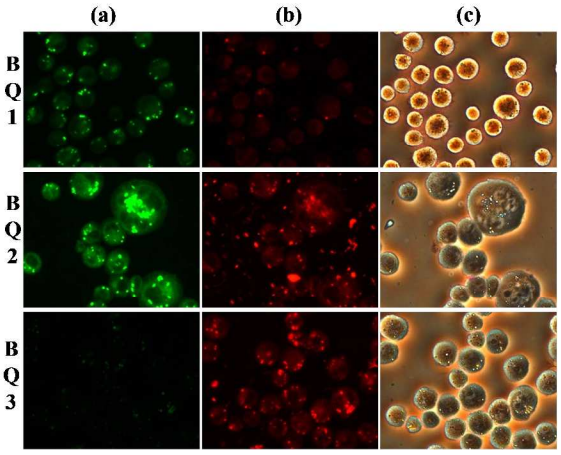

Fig. 5 (a, b) Fluorescent and (c) bright field images of DL cells stained with **BQ1**–**BQ3**.

The efficacy of these luminogens in biological systems has been explored by live cell imaging experiments. DL cells were incubated with **BQ1**–**BQ3** for 2 h and co-stained with Hoechst 33342 to identify nuclear region of the cells. These compounds stained cytoplasm

ChemComm Accepted Manuscript

excluding the nucleus (Fig. S35, ESI†). All the compounds showed dichromic (green and red) fluorescence under blue or green excitation (Fig. 5) due to presence of both monomeric and aggregated species. The endocytosis is believed to be major route for internalization of compounds. Noticeably, the green emission was weakest in **BQ3** while **BQ1** displayed faint red emission owing to their variable extents of aggregation. Thus these compounds may be potentially useful in studying the endocytic structures and pathways.

Conclusions

In conclusion, three novel quinoline-BODIPY based systems (**BQ1**-–**BQ3**) have been designed and synthesized. AIE in these compounds is triggered under direct influence of steric hindrance on RIR. This approach relies on simplifying fine tuning of the nanoaggregate morphology through minimum possible changes in substituents from –H, $–CH_3$ to $–OCH_3$. Two types of aggregates *viz.* spherical (**BQ1, BQ2**) and fibrous (**BQ3**) were obtained from the same platform. Vital role of the substituents has also been rationalized from photophysical properties and crystal packing patterns. The AIE phenomenon has been explored in live cell imaging and a dichromic (red/green) fluorescence in DL cells has been visualized. Further elaboration of this approach may lead to aggregates with desired shape and properties.

We acknowledge financial support from the Department of Science and Technology (DST), New Delhi through the Scheme SR/S1/IC-25/2011. RSS acknowledges the University Grants Commission, New Delhi, India for a Senior Research Fellowship (19-12/2010(i) EU-IV).

Notes and references

[a]Department of Chemistry, Faculty of Science, Banaras Hindu University, Varanasi - 221 005 (U.P.) India.
[b]Department of Zoology, Faculty of Science, Banaras Hindu University, Varanasi - 221 005 (U.P.) India.

†Electronic Supplementary Information (ESI) available: Synthetic procedures, chemical compound information, XRD data (CIF), Absorption, fluorescence studies and theoretical calculations. CCDC 1039757–1039760. For ESI and crystallographic data in CIF or other electronic format see DOI: 10.1039/c000000x/

1 (a) J. Luo, Z. Xie, J. W. Y. Lam, L. Cheng, H. Chen, C. Qiu, H. S. Kwok, X. Zhan, Y. Liu, D. Zhu and B. Z. Tang, *Chem. Commun.*, 2001, 1740–1741; (b) Y. Hong, J. W. Y. Lam and B. Z. Tang, *Chem. Soc. Rev.*, 2011, **40**, 5361–5388.

2 (a) R. Hu, C. F. A. G-Durán, J. W. Y. Lam, J. L. B-Vázquez, C. Deng, S. Chen, R. Ye, P. E. Cabrera, Y. Zhong, K. S. Wong and B. Z. Tang, *Chem. Commun.*, 2012, **48**, 10099–10101; (b) G. Iasilli, A. Battisti, F. Tantussi, F. Fuso, M. Allegrini, G. Ruggeri and A. Pucci, *Macromol. Chem. Phys.*, 2014, **215**, 499−506; (c) S. S. Palayangoda, X. Cai, R. M. Adhikari and D. C. Neckers, *Org. Lett.*, 2008, **10**, 281–284; (d) R. Misra, T. Jadhav, B. Dhokale and S. M. Mobin, *Chem Commun.*, 2014, **50**, 9076–9078.

3 (a) P. Galer, R. C. Korošec, M. Vidmar and B. Šket, *J. Am. Chem. Soc.*, 2014, **136**, 7383−7394; (b) L. Wang, W. Li, J. Lu, Y. X. Zhao, G. Fan, J. P. Zhang and H. Wang, *J. Phys. Chem. C*, 2013, **117**, 26811−26820; (c) T. He, X. T. Tao, J. X. Yang, D. Guo, H. B. Xia, J. Jia and M. H. Jiang, *Chem. Commun.*, 2011, **47**, 2907–2909; (d) C. W. Liao, M. R. Rao and S. S. Sun, *Chem. Commun.*, 2015, **51**, 2656–2659.

4 (a) X. Wang , J. Hu , G. Zhang , S. Liu, *J. Am. Chem. Soc.*, 2014, **136**, 9890–9893; (b) R. T. K. Kwok, C. W. T. Leung, J. W. Y. Lam, B. Z. Tang, *Chem. Soc. Rev.*, 2015, *DOI: 10.1039/C4CS00325J*; (c) K. Wang, X. Zhang, X. Zhang, B. Yang, Z. Li, Q. Zhang, Z. Huang, Y. Wei, *Polym. Chem.*, 2015, **6**, 1360-1366.

5 (a) J. Iehl, J. F. Nierengarten, A. Harriman, T. Bura and R. Ziessel, *J. Am. Chem. Soc.*, 2012, **134**, 988–998; (b) R. Ziessel, B. D. Allen, D. B. Rewinska and A. Harriman, *Chem.−Eur. J.*, 2009, **15**, 7382−7393; (c) F. Li, S. I. Yang, Y. Ciringh, J. Seth, C. H. Martin III, D. L. Singh, D. Kim, R. R. Birge, D. F. Bocian, D. Holten and J. S. Lindsey, *J. Am. Chem. Soc.*, 1998, **120**, 10001–10017; (d) H. Sunahara, Y. Urano, H. Kojima and T. Nagano, *J. Am. Chem. Soc.*, 2007, **129**, 5597−5604; (e) S. S. Ragab, S. Swaminathan, J. D. Baker and F. M. Raymo, *Phys. Chem. Chem. Phys.*, 2013, **15**, 14851−14855.

6 (a) T. T. Vu, S. Badre, C. D. Verdes, J. J. Vachon, C. Julien, P. Audebert, E. Y. Senotrusova, E. Y. Schmidt, B. A. Trofimov, R. B. Pansu, G. Clavier and R. M. Renault, *J. Phys. Chem.* C, 2009, **113**, 11844–11855; (b) S. Mukherjee and P. Thilagar, *Chem.− Eur. J.*, 2014, **20**, 9052 –9062; (c) S. Choi, J. Bouffard and Y. Kim, *Chem. Sci.*, 2014, **5**, 751–755.

7 (a) W. Li, W. Lin, J. Wang and X. Guan, *Org. Lett.*, 2013, **15**, 1768–1771; (b) M. W. Chung, T. Y. Lin, C. C. Hsieh, K. C. Tang, H. S. Fu, P. T. Chou, S. H. Yang and Y. Chi, *J. Phys. Chem. A*, 2010, **114**, 7886–7891.

8 (a) Y. Mikata, Y. Sato, S. Takeuchi, Y. Kuroda, H. Konno and S. Iwatsuki, *Dalton Trans.*, 2013, **42**, 9688–9698; (b) X. Zhou, P. Li, Z. Shi, X. Tang, C. Chen and W. Liu, *Inorg. Chem.*, 2012, **51**, 9226–9231; (c) X. Meng, S. Wang, Y. Li, M. Zhu and Q. Guob, *Chem. Commun.*, 2012, **48**, 4196–4198; (d) M. Rouffet, C. A. F. D. Oliveira, Y. Udi, A. Agrawal, I. Sagi, J. A. McCammon and S. M. Cohen, *J. Am. Chem. Soc.*, 2010, **132**, 8232–8233.

9 A. Shao, Z. Guo, S. Zhu, S. Zhu, P. Shi, H. Tiana and W. Zhu, *Chem. Sci.*, 2014, **5**, 1383-1389.

10 R. S. Singh, M. Yadav, R. K. Gupta, R. Pandey and D. S. Pandey, *Dalton Trans.*, 2013, **42**, 1696–1707.

11 R. Hu, E. Lager, A. A. Aguilar, J. Liu, J. W. Y. Lam, H. H. Y. Sung, I. D. Williams, Y. Zhong, K. S. Wong, E. P. Cabrera and B. Z. Tang, *J. Phys. Chem. C*, 2009, **113**, 15845–15853.

ChemComm Accepted Manuscript

 This journal is © The Royal Society of Chemistry 2012